nature chemistry

ARTICLES

PUBLISHED ONLINE: 23 JANUARY 2011 | DOI: 10.1038/NCHEM.961

Single cells and intracellular processes studied by a plasmonic-based electrochemical impedance microscopy

Wei Wang, Kyle Foley, Xiaonan Shan, Shaopeng Wang, Seron Eaton, Vinay J. Nagaraj, Peter Wiktor, Urmez Patel and Nongjian Tao*

Electrochemical impedance spectroscopy is a crucial tool for the detection and study of various biological substances, from DNA and proteins to viruses and bacteria. It does not require any labelling species, and methods based on it have been developed to study cellular processes (such as cell spreading, adhesion, invasion, toxicology and mobility). However, data have so far lacked spatial information, which is essential for investigating heterogeneous processes and imaging high-throughput microarrays. Here, we report an electrochemical impedance microscope based on surface plasmon resonance that resolves local impedance with submicrometre spatial resolution. We have used an electrochemical impedance microscope to monitor the dynamics of cellular processes (apoptosis and electroporation of individual cells) with millisecond time resolution. The high spatial and temporal resolution makes it possible to study individual cells, but also resolve subcellular structures and processes without labels, and with excellent detection sensitivity (~2 pS). We also describe a model that simulates cellular and electrochemical impedance microscope images based on local dielectric constant and conductivity.

Continued advances in science depend critically on the development of new enabling spectroscopic and microscopic tools. One important example is electrochemical impedance spectroscopy (EIS). The basic working principle of EIS is to apply an a.c. voltage (ΔV) to an electrode and monitor the current response (ΔI). Impedance Z (determined by $Z = \Delta V/\Delta I$) is sensitive to processes such as a molecular binding event and apoptosis of cells taking place on the electrode surface. This technique has been developed to study and detect various biological substances, from DNA and proteins to viruses and bacteria[1,2], without the need for labelling species. Giaever and colleagues[3,4] have pioneered an EIS method to study many cellular processes, including cell spreading, adhesion, invasion, toxicology and motility.

Although powerful, conventional EIS lacks spatial information, which is essential for studying heterogeneous processes and for imaging high-throughput microarrays. For example, the study of cellular heterogeneity, a particularly important area of research, demands new tools for single cell analysis[5,6]. To obtain spatial information one could, in principle, use an array of microelectrodes[7–9], each providing an impedance signal at a particular location. However, high spatial resolution would require a high-density array of microelectrodes, which would demand sophisticated microfabrication techniques and complex interconnection and multiplexing of the microelectrodes[10]. Because electrochemical current scales with the size of the microelectrode, increasing spatial resolution by shrinking the microelectrodes results in a decreasing impedance signal measured by each microelectrode, and the measurement is susceptible to unwanted electronic interference between the closely spaced microelectrodes. For these reasons, high-resolution impedance microscopy using microelectrodes is not yet possible.

An alternative approach to obtaining spatial resolution is to measure the impedance between a microelectrode and a surface by mechanically scanning the microelectrode across the sample[11,12]. In this approach, however, the measured impedance depends not only on the sample properties but also the impedance of the microelectrode, which complicates interpretation of the data[13]. Furthermore, the mechanically scanning tip is slow and may introduce perturbation in the measurements.

Here, we present an electrochemical impedance microscope (EIM) that can optically resolve local impedance with a submicrometre spatial resolution without using microelectrodes, which overcomes the difficulties of conventional impedance measurements. This also allows for simultaneous optical and surface plasmon resonance (SPR) imaging of the same sample, providing additional and complementary information. Using the EIM, we have monitored various processes, such as apoptosis and electroporation of cells, with millisecond time resolution. The high spatial and temporal resolution images make it possible not only to study individual cells, but also to resolve subcellular structures and processes without using labels.

Unlike conventional EIS, which measures electrochemical current, operation of the EIM is based on the sensitive dependence of SPR on surface charge density, which is measured optically (Fig. 1a), thus allowing for fast and non-invasive imaging of impedance. The EIM maps the local electrical polarizability and conductivity, reflecting local changes in cellular structure and ionic distribution—important information that is not available using other microscopes. The EIM developed in this study relies on detecting surface plasmon waves propagating on a metal thin film. The surface plasmon waves are created by a laser beam incident on the metal film, typically via a prism at a so-called resonant angle, and the reflected beam creates an SPR image. The resonant angle is known to be sensitive to changes in refractive index near the metal surface; this has been widely used to study molecular

Center for Bioelectronics and Biosensors, Biodesign Institute, Department of Electrical Engineering, Arizona State University, Tempe, Arizona 85287, USA.
*e-mail: njtao@asu.edu

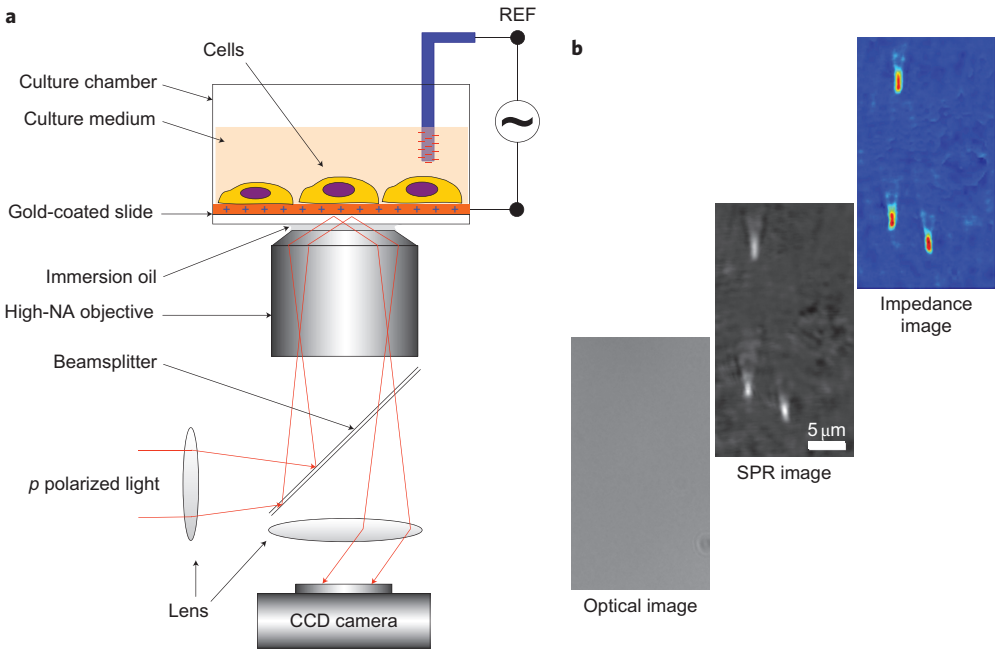

Figure 1 | Electrochemical impedance microscopy. a, Schematic of the experimental setup. A laser beam (polarized light) is directed by lenses onto a gold-coated glass coverslip through an oil immersion high-NA (numeric aperture) objective to create SPR on the gold surface, which is imaged with a CCD camera. Cells are cultured for study on the gold-coated cover glass. An a.c. modulation potential is applied to the gold electrode relative to a reference electrode (REF) inserted in the culture medium solution. The EIM image is created from the potential-induced SPR signal changes. In addition to the SPR and EIM images, a conventional optical image of the same sample can also be recorded. **b**, Examples of optical, SPR and EIM images of 200 nm silica nanoparticles, demonstrating the spatial resolution of the systems. The optical image cannot resolve the nanoparticles. The SPR image shows each nanoparticle as a bright spot with a long tail in the SPR propagation direction. The EIM image has similar spatial resolution to the SPR image.

binding processes[14,15] and, more recently, to image electrochemical current[16]. In contrast, the EIM is based on the sensitive dependence of SPR on surface charge density.

In the same way as for conventional EIS, we apply an a.c. voltage to the surface to create a surface charge density modulation (Δq), which induces a SPR signal change ($\Delta\theta$). We have previously shown that the charge density q of a surface is related to the SPR signal θ by $\Delta q(x,y,\omega) = \alpha\Delta\theta(x,y,\omega)$, where ω is the angular frequency of the a.c. modulation, x and y denote a location on the electrode, and $\alpha \approx 28$ C m^{-2} deg^{-1} is a constant that can be determined either by experimental calibration or calculation[17]. From the surface charge density distribution, we then determine the local impedance Z of the surface using

$$Z^{-1}(x, y, \omega) = j\omega\alpha\Delta\theta(x, y, \omega)/\Delta V \qquad (1)$$

where $j = \sqrt{-1}$ and ΔV is the amplitude of the applied voltage modulation. This equation arises from the fact that current density is the rate of change of the surface charge density J, given by $J = \mathrm{d}q/\mathrm{d}t$, and $q = q_0\exp(-j\omega t)$, where q_0 is the amplitude of the surface charge density modulation induced by the voltage modulation.

In our previous work[17] we used a conventional SPR setup to demonstrate the possibility of measuring the surface charge of a bare gold and self-assembled monolayer with static SPR, and the finding was modelled in terms of capacitors and resistors. However, as SPR can only probe an area of ~200 nm near the surface, and because the capacitor–resistor model is inadequate for describing a heterogeneous sample, whether the SPR-based method can be applied to thick and heterogeneous samples such as cells has remained questionable. Furthermore, the spatial resolution of the conventional prism SPR setup was insufficient to resolve single cells. In the present work, we have now developed a new impedance imaging capability with submicrometre spatial resolution, as well as a signal-processing algorithm for fast video analysis, which makes it possible to image single cells. More importantly, we show that the impedance imaging method works for thick and heterogeneous samples, and we have developed a microscopic model based on local electrical polarizability and conductivity. This not only validates the concept, but also provides a foundation for future impedance imaging of heterogeneous samples. Finally, we demonstrate that the new imaging technique can indeed be applied to image and study subcellular processes, apoptosis and electroporation.

Results and discussion

Single cell detachment and numerical simulation. Figure 2 shows optical, SPR and EIM images of a cultured human cervical cancer cell from the SiHa cell line undergoing early apoptosis, recorded simultaneously with an EIM. The EIM image contrast was found to be inversely proportional to the impedance (that is, directly proportional to the admittance, $1/Z$). This demonstrates that EIM can resolve not only individual cells but also subcellular structures; for example, the nucleolus of the cell (a substructure of the nucleus composed of proteins and nucleic acids) appears on the EIM image as a dark spot (marked by a black arrow in Fig. 2). Conventional EIS measures an average impedance response over many cells on an electrode. Typically this would be modelled using a combination of resistors and capacitors, and the data were often displayed graphically as Bode or Nyquist plots[18,19]. This means that the conventional model treats cells as cylindrical disks described by a few simple parameters; this is useful for interpretation of EIS data, but not for resolution of the internal structure of each cell, which requires a microscopic model accounting for local differences rather than averages.

In the present EIM setup, impedance measures the response of the cells to a small external electrical field. This can be modelled in terms of local polarizability and conductivity σ of the cell and

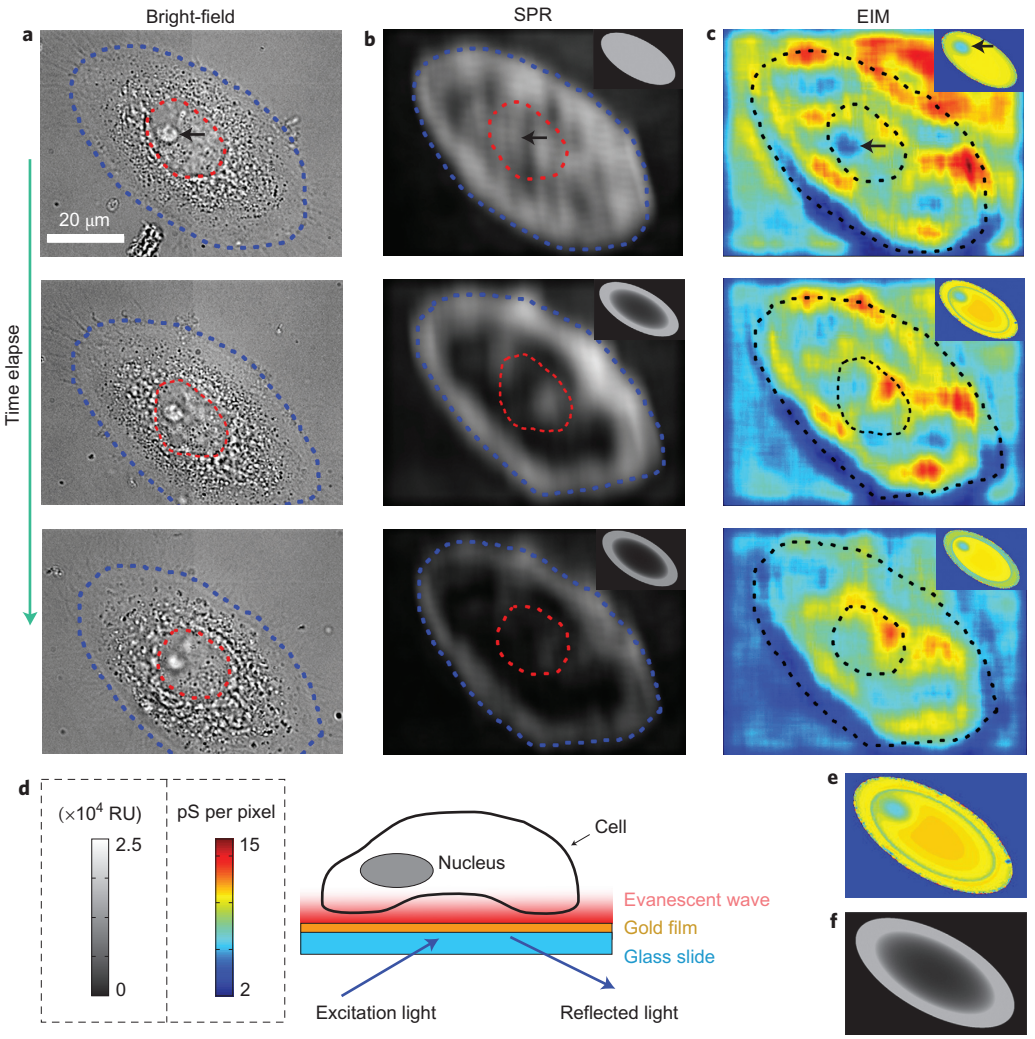

Figure 2 | Impedance images of a single cell and model simulation. a–c, Simultaneously recorded optical transmission (**a**), SPR (**b**) and EIM (**c**) images of a SiHa cell at 0 min (top), 30 min (middle) and 75 min (bottom) after apoptosis treatment. The insets in **b** and **c** show simulated SPR and EIM images. **d**, Schematic illustration of SPR imaging, showing that an evanescent field localized near the surface interacts with the bottom portion of a cell. The evanescent wave is an exponentially decaying wave at the glass–gold interface. **e**,**f**, Simulated EIM (**e**) and SPR (**f**) images that reproduce the main features observed in the experimental images. Red dashed circles outline the cell nucleus; blue dashed circles outline the cell (these are both shown in black in **c** for clarity); black arrows indicate the nucleolus of the cell. The grey scale bar represents the *z*-axis scale of SPR with units of response unit (RU), where black indicates zero RU and white is 2.5×10^4 RU. The colour scale bar is the *z*-axis scale of EIM with units of pS per pixel, where dark blue indicates 2 pS per pixel and red is 15 pS per pixel. The size of a single pixel is ~0.0625 μm^2 (0.25 μm × 0.25 μm).

surrounding environment. The polarizability (quantified by the local dielectric constant, ε_r) describes the non-conductive regions, such as membranes, and the conductivity describes the ionic conduction. In a given region, both contributions may co-exist. This is described by a complex permittivity $\varepsilon = \varepsilon_0\varepsilon_r + j\sigma/\omega$, where ε_0 is the permittivity of vacuum. The real and imaginary parts of the permittivity correspond to the capacitive and resistive components, respectively, in conventional impedance models. The EIM image therefore maps local variations in the dielectric and conductive properties, which in turn reflect changes in the cellular structure and ionic distribution, respectively. Such information is important for a better understanding of various cellular processes, but is not available from existing microscopes.

To further illustrate that local variations in the local polarizability and conductivity lead to a change in the EIM image contrast, we have numerically simulated the EIM of a cell attached to a surface. The simulation setup includes a bottom electrode on which a cell is attached, a buffer medium and a top electrode. A voltage between the top and bottom electrodes provides a weak electric field, and the local SPR response of the bottom electrode is used to create an EIM image. The model cell contains a cell membrane, cytoplasm and a nucleus and its envelope (Fig. 2d; see Supplementary Information for more details). Although this model is simplified, it contains more structural details than the existing EIS models of cells, and can be expanded to include more details when needed. Figure 2e shows a simulated EIM image, which captures the variations in the dielectric constant and conductivity in the cell. For comparison, a simulated SPR image based on the same model is shown in Fig. 2f.

Although the main goal of the present work is to demonstrate real-time imaging of single cells using the EIM, we have also explored the capability of the new microscopy for monitoring cellular processes. Among the various cellular processes, the study of apoptosis (a programmed cell death process) is of paramount importance due to its critical role in homeostasis, tissue/organ development and diseases such as cancer. Cancer results from the loss of cellular mechanisms that regulate apoptosis, and cancer therapy strategies therefore frequently rely on the induction of

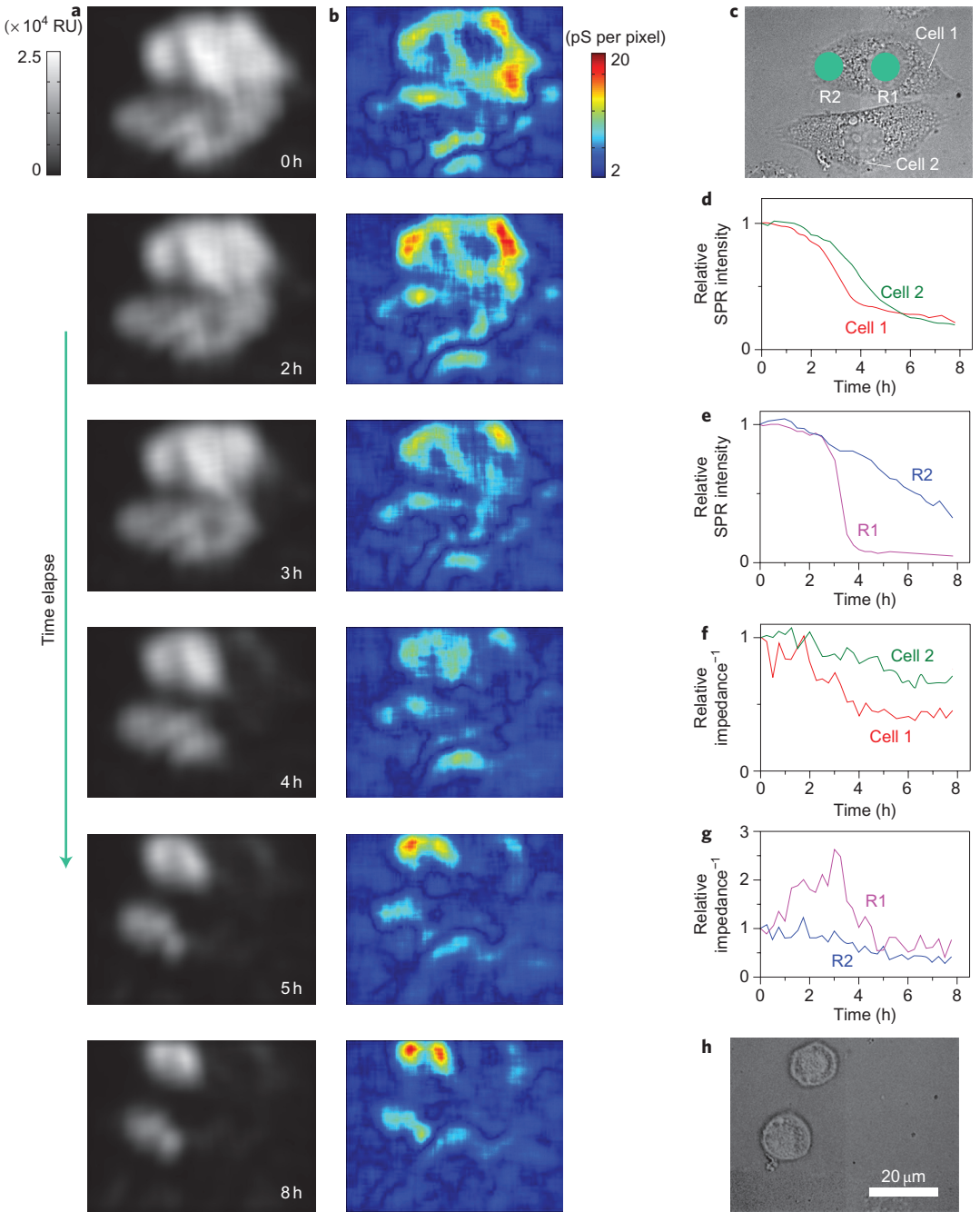

Figure 3 | Monitoring single cell apoptosis with EIM. a,**b**, Sequence of snapshots of apoptotic events in SiHa cells, illustrating time-dependent SPR (**a**) and EIM images (**b**). **c**,**h**, Bright-field optical images before (**c**) and after (**h**) apoptosis, showing changes in morphology. **d**–**g**, Quantitative profiles of SPR (**d**,**e**) and EIM (**f**,**g**) are analysed for individual cells (**d**,**f**) and subcellular regions (**e**,**g**) within a single cell. The grey scale bar represents the *z*-axis scale of SPR with units of RU, where black indicates zero RU and white is 2.5×10^4 RU. The colour scale bar represents the *z*-axis scale of EIM with units of pS per pixel, where dark blue is 2 pS per pixel and red is 20 pS per pixel. The size of a single pixel is $\sim 0.0625\ \mu m^2$ ($0.25\ \mu m \times 0.25\ \mu m$).

apoptosis in malignant cells[20]. The induction and progression of cellular apoptotic events in the cervical cultured cancer SiHa cells were investigated using EIM. Cell death by apoptosis can be induced in SiHa cells by treatment with MG132 (a molecule that inhibits the proteosome) in combination with the protein TRAIL (tumour necrosis factor-related apoptosis-inducing ligand)[21]. Exposure of SiHa cells to MG132 and TRAIL results in changes typical of apoptosis, including cellular shrinking, condensation followed by fragmentation of the nuclear material, formation of blebs at the plasma membrane, and eventual disintegration of the cells into several membrane-bound apoptotic bodies.

The optical, SPR and EIM images recorded simultaneously provide rich and complementary information about the cellular processes during apoptosis. Conventional bright-field optical imaging is well established, and serves as a reference technique. The SPR image resolves the bottom portion ($\sim$200 nm) of the cell on the surface, and is therefore particularly useful for studying cell–surface interactions. As shown by the images in Fig. 2b, apoptosis starts with a decrease in SPR image brightness near the centre of the cell, reflecting detachment of the cell from the surface, starting from the centre. This detachment process is not resolved in the conventional optical image (Fig. 2a), but the EIM images (Fig. 2c) taken

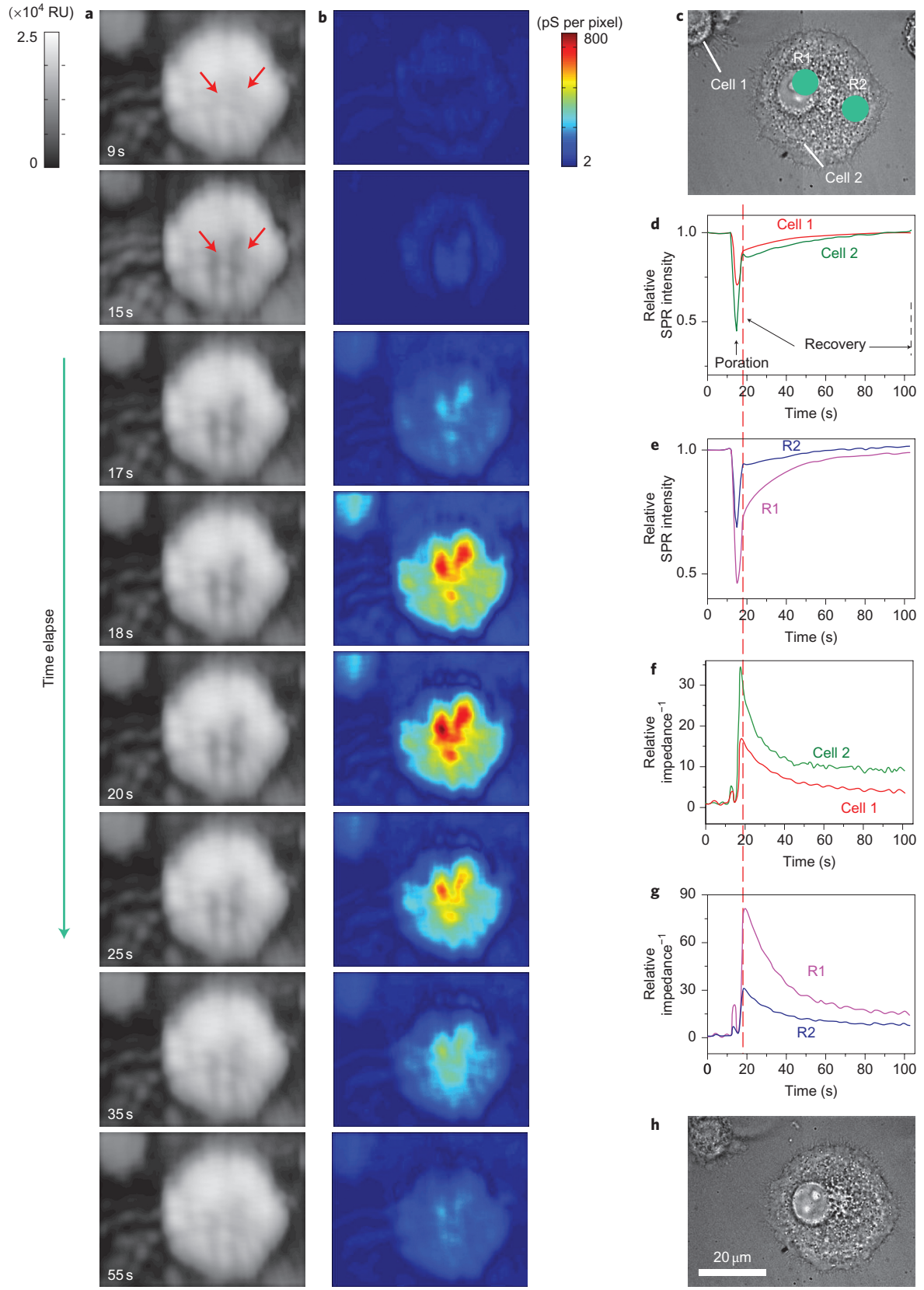

Figure 4 | Monitoring single cell electroporation with EIM. a,**b**, Time-dependent SPR (**a**) and EIM images (**b**) during an electroporation process. The regions marked by a red arrow show a large decrease in brightness on electroporation. This indicates a local detachment of the cell membrane from the surface. **c**,**h**, Bright-field optical images before (**c**) and after (**h**) electroporation, showing changes in morphology. **d**–**g**, Quantitative profiles of SPR (**d**,**e**) and EIM (**f**,**g**) are analysed for individual cells (**d**,**f**) and subcellular regions (**e**,**g**) within a single cell. The grey scale bar is the *z*-axis scale of SPR with units of RU, where black represents zero RU and white is 2.5×10^4 RU. The colour scale bar represents the *z*-axis scale of EIM with units of pS per pixel, where dark blue is 2 pS per pixel and red is 800 pS per pixel. The size of a single pixel is ~0.0625 μm^2 (0.25 $\mu m \times 0.25$ μm).

simultaneously show large and dynamic changes in the cell during apoptosis. For example, the nucleolus region changes rapidly in the EIM images (but not in the conventional optical image). Previously, investigation of such changes to a nucleolus was possible only through fluorescent staining or by using electron microscopy. The region indicated by the black arrow shows a large increase in image intensity, which is not resolved by either the optical image or the SPR image. Based on the model described above, we simulated both SPR (insets in Fig. 2b) and EIM (insets in Fig. 2c) images during apoptosis. The simulated SPR image reproduces the observed decrease in brightness starting from the cell centre (see Supplementary Information). The simulated EIM image reproduces the basic features of the measured image, including the decrease in contrast of the nucleolus.

Apoptosis. A more convenient way to view the wealth of information from EIM is by video. Figure 3 shows a sequence of snapshots from SPR (Fig. 3a) and EIM (Fig. 3b) videos of two cells during apoptosis (Supplementary Movie S1). For comparison, conventional optical images of the cells recorded in the beginning (Fig. 3c) and last stages (Fig. 3h) of apoptosis are also shown. By selecting different regions of the images, quantitative local and total impedance information versus time can be readily obtained. For example, by selecting the entire region of each cell, the total impedance responses of the two cells as a function of time can be analysed (Fig. 3f). Although the impedance responses of both cells decrease with time, they occur at different rates, reflecting heterogeneity of cell apoptosis, which underscores the importance of single cell analysis. Decreases in the total impedance responses of the two cells are mainly due to detachment of the cells from the electrode surface, which is evident from the SPR and optical images. In fact, the total SPR image intensities of the two cells versus time show a similar behaviour (Fig. 3d).

By selecting different regions within a cell, one can also follow the change in impedance of a particular region of interest. Figure 3g plots the impedance responses of the nucleus region and an adjacent region of Cell 1. The response of the nucleus region of Cell 1 (marked R1 in Fig. 3c) increases initially, then decreases after reaching a peak. This is in contrast to the response of the adjacent region (marked R2 in Fig. 3c), which decreases monotonically. The corresponding time profiles of the two selected regions of the SPR images are plotted in Fig. 3e, illustrating the different responses of the two regions. For Region 2, the SPR signal decreases smoothly, which is comparable to the EIM response. In contrast, for Region 1, the SPR signal drops suddenly when the EIM response reaches the maximum. The different responses of Cells 1 and 2, and local regions R1 and R2 within Cell 1 are a result of heterogeneous cellular apoptosis processes that have been resolved by the EIM.

Electroporation. We have also applied the EIM to study electroporation, a process that has been used for introducing DNA and drugs into cells[22,23]. Electroporation can be triggered by applying a voltage pulse to a cell, which creates large increases in the electrical conductivity and permeability of the cell plasma membranes[24]. We recorded EIM images (together with optical and SPR images) of electroporation processes. Figure 4 shows a sequence of snapshots of an electroporation process (for a complete video of the process see Supplementary Movie S2). The optical image shows few changes during and after the electroporation process, as shown in Fig. 4c and h, respectively, whereas the SPR image reveals a large change during the process. For example, the regions marked by red arrows in Fig. 4a show a relatively large decrease in brightness when an electroporation potential is applied for 3 s, indicating local detachment of the cell membrane from the surface. However, the SPR image recovers after the large transient change within a minute. The EIM image shows the most dramatic changes. It starts with a large and rapid increase in the impedance response, followed by a recovery process much slower than the SPR image.

The time-dependent profiles of particular regions show more clearly the changes in the SPR and impedance images. The SPR profile of the cellular region (red and green in Fig. 4d) shows a large negative response, which recovers over ~60 s. Note that SPR signal recovery is complete, which is similar to the results for conventional optical images (Fig. 4c,h). Time-dependent profiles for the corresponding regions using the EIM are shown in Fig. 4f,g. In sharp contrast to the SPR and optical images, the impedance signal of the cellular region shows a large increase and is then followed by a slow decay. The large change in impedance signal is expected during the electroporation process, because it creates openings in the cell membranes. The change is not uniform across the entire cell. For example, the SPR and impedance signals from two selected regions, marked R1 and R2, are shown in Fig. 4c. It is clear that both the SPR and impedance responses for Region 1 are much larger than those of Region 2. Unlike the optical and SPR images, the impedance signal of the cell does not fully recover its initial value. We believe that the residual change is due to a slow recovery process, because, according to a previous report[24], the complete electroporation healing of cells attached to a gold surface usually takes several hours.

The spatial resolution of the EIM along the direction of surface plasmon waves is determined by the plasmon propagation distance, which depends on the electrode material and wavelength of incident light. For a gold electrode in aqueous solutions, the spatial resolution along the plasmon waves is ~3 μm using 635 nm light. Figure 1b shows the impedance image of a 200 nm silica nanoparticle. However, when using 532 nm light, the resolution improves to ~0.2 μm. Perpendicular to the plasmon propagation direction, the resolution is determined by the diffraction limit. Using a numerical aperture of 1.65, the diffraction limit is ~0.2 μm. The detection limit of the local impedance also depends on several factors, including the amplitude and frequency of applied voltage modulation, light source, camera, and thermal and mechanical noises. In the present system, the detection limit in terms of admittance (inverse of impedance) is ~2 pS (assuming a modulation amplitude of 0.1 V, modulation frequency of 170 Hz, wavelength of 635 nm), which is excellent, considering that the conductance of a single ion channel is between 5 and 400 ps. The frequency range of the EIM is determined by camera speed, which has a maximum frame rate of 380 frames per second in our setup. In the present work, we imaged cells as a function of time at fixed frequencies. A fast charge-coupled device (CCD) with a frame rate in the range of megahertz is available; this can speed up the EIM to enable the detection of extremely fast events. This will also make it possible to acquire EIM images by scanning the frequency over a wide range to obtain additional information. Finally we point out that, unlike with fluorescence imaging, the temporal resolution of SPR-based EIM imaging is not limited by the light emitting intensity.

We have demonstrated an EIM that images structural and ionic distribution changes in individual adherent cultured mammalian cells. The EIM is label-free, non-invasive, has high spatial and temporal resolutions, and provides local impedance information that was not previously available. Further systematic studies will help to develop a microscopic model that relates various cellular processes to local conductivity and dielectric responses, and interpret the data obtained with widely used EIS measurements of cells. We also anticipate that the new EIM will have broad applications in research related to drug discovery for cancer therapy and other diseases, host cell–pathogen interactions, differentiation of stem cells, as well as studies involving label-free interactions of biomolecules such as DNA, proteins, enzymes, sugars and lipids using microarrays.

Methods

Cell culture. The human cervical cell line SiHa was purchased from the American Type Culture Collection. SiHa cells were cultured in a humidified atmosphere at 37 °C with 5% CO_2 and 70% relative humidity. Cells were grown in Dulbecco's modified eagle's medium (DMEM, Invitrogen) with 10% fetal bovine serum (FBS, Invitrogen) with penicillin and streptomycin (BioWhittaker). Cells were passaged with 0.05% trypsin and 0.02% ethylenediamine-tetraacetic acid (EDTA) in Hank's balanced salt solution (HBSS, Sigma-Aldrich) when they reached a confluency of ~75%.

Impedance measurements. The imaging setup was based on an objective-based inverted microscope system introduced by Zare and colleagues[25]. The optical system comprised a He–Ne laser source (633 nm), an optical fibre, an inverted microscope (Olympus X81) and a CCD camera (Pike F-032). The sensor chip was a BK7 glass coverslip coated with ~2 nm of chromium followed by ~47 nm of gold. Before use, each chip was washed with water and ethanol, followed by hydrogen flame-annealing to remove surface contamination. A Flexi-Perm silicon chamber (Greiner Bio-One) was placed on top of the gold chip and acted as both cell culture well and electrochemical cell. The potential of the sensor surface was controlled with respect to a silver-wire quasi-reference electrode with a bipotentiostat (Pine ARFDE5) and platinum-wire counter-electrode. Modulation with a frequency of 170 Hz and amplitude up to 150 mV was applied using an external function generator. We also applied a lower-amplitude modulation, which produced more noisy but similar images for the samples studied in this work (surface covered with a layer of molecules).

To seed SiHa cells on the gold chip, 200 μl of growth medium with 5,000 cells was added to a FlexiPerm well attached to the chip. The seeded chips were placed in an enclosed culture chamber (Tokaihit INU-ONICS-F1) on the microscope platform with controlled conditions (temperature of 37 °C, 5% CO_2 and 75% relative humidity). After overnight incubation, the cells adhered to the gold surface and spread out. Controlled conditions were maintained throughout the experiment.

Apoptosis and electroporation. To induce apoptosis, 10 μM proteosome inhibitor MG132 (Sigma) was added and incubated for 2 h, then 1 μg ml^{-1} of human recombinant TRAIL (Calbiochem/EMD Biochemicals) consisting of the amino-acid sequence 114–281 was added before EIM measurements. For electroporation, 1 MHz a.c. modulation with a V_{pp} of 20 V was applied on the electrode for a duration time of 3 s.

Video processing. Postprocessing of data was accomplished using a program written in Matlab. A 25-point two-dimensional finite impulse response filter was applied to each image to minimize the intensity fluctuation for a single pixel. The sampling time of the fast Fourier transform (FFT) process was 2 s. Typically, when the camera frame rate was 380 frames per second, 760 filtered images were processed pixel-by-pixel by FFT to create an amplitude image and an averaged SPR image. SPR video and EIM video were constructed from a series of averaged SPR images and amplitude images at different times, respectively.

EIM and SPR image modelling. The EIM was modelled using COMSOL, a multiphysics modelling and simulation package that solves Maxwell's equations with appropriate boundary conditions. The cell was modelled as a hemispherical structure attached to the gold electrode. The model cell included a membrane, cytoplasm medium, a nucleus and its envelope, each with different dielectric constants and conductivities ($\varepsilon = 6.2$, 60, 28 and 52; $\sigma = 0.169$, 0.5, 0.01 and 1.35 S m^{-1} for the membrane, cytoplasm, nucleus envelope and nucleus, respectively). The simulation also assumed that the buffer medium had a dielectric constant of 79 and a conductivity of 1.69 S m^{-1}. Solving Maxwell's equations numerically, we could obtain the electric field near the bottom electrode, from which the local surface charge density modulation Δq could be obtained. The EIM image was obtained based on $Z^{-1} = j\omega\Delta q/\Delta V$. The SPR simulation was carried out using $n(x,y,z)e^{-z/l}$, where $n(x,y,z)$ is the local refractive index of the cell and surrounding medium, and the exponential term reflects the decay of the evanescent field (decay length, $l \approx 200$ nm).

Received 6 August 2010; accepted 29 November 2010; published online 23 January 2011

References

1. Katz, E. & Willner, I. Probing biomolecular interactions at conductive and semiconductive surfaces by impedance spectroscopy: routes to impedimetric immunosensors, DNA-sensors, and enzyme biosensors. *Electroanal.* **15,** 913–947 (2003).
2. Maalouf, R. *et al.* Label-free detection of bacteria by electrochemical impedance spectroscopy: comparison to surface plasmon resonance. *Anal. Chem.* **79,** 4879–4886 (2007).
3. Giaever, I. & Keese, C. R. A morphological biosensor for mammalian cells. *Nature* **366,** 591–592 (1993).
4. Giaever, I. & Keese, C. R. Monitoring fibroblast behavior in tissue-culture with an applied electric field. *Proc. Natl Acad. Sci. USA* **81,** 3761–3764 (1984).
5. Slack, M. D., Martinez, E. D., Wu, L. F. & Altschuler, S. J. Characterizing heterogeneous cellular responses to perturbations. *Proc. Natl Acad. Sci. USA* **105,** 19306–19311 (2008).
6. Schulte, A. & Schuhmann, W. Single-cell microelectrochemistry. *Angew. Chem. Int. Ed.* **46,** 8760–8777 (2007).
7. Rothermel, A. *et al.* Real-time measurement of PMA-induced cellular alterations by microelectrode array-based impedance spectroscopy. *BioTechniques* **41,** 445–450 (2006).
8. Rahman, A. R. A., Register, J., Vuppala, G. & Bhansali, S. Cell culture monitoring by impedance mapping using a multielectrode scanning impedance spectroscopy system (CellMap). *Physiol. Meas.* **29,** S227–S239 (2008).
9. Chai, K. T. C., Davies, J. H. & Cumming, D. R. S. Electrical impedance tomography for sensing with integrated microelectrodes on a CMOS microchip. *Sens. Actuators B* **127,** 97–101 (2007).
10. Lin, Z., Ino, K., Shiku, H. & Matsue, T. Electrochemical topography of a cell monolayer with an addressable microelectrode array. *Chem. Commun.* **46,** 559–561 (2010).
11. Alpuche-Aviles, M. A. & Wipf, D. O. Impedance feedback control for scanning electrochemical microscopy. *Anal. Chem.* **73,** 4873–4881 (2001).
12. Katemann, B. B., Schulte, A., Calvo, E. J., Koudelka-Hep, M. & Schuhmann, W. Localised electrochemical impedance spectroscopy with high lateral resolution by means of alternating current scanning electrochemical microscopy. *Electrochem. Commun.* **4,** 134–138 (2002).
13. Ervin, E. N., White, H. S. & Baker, L. A. Alternating current impedance imaging of membrane pores using scanning electrochemical microscopy. *Anal. Chem.* **77,** 5564–5569 (2005).
14. Rothenhausler, B. & Knoll, W. Surface-plasmon microscopy. *Nature* **332,** 615–617 (1988).
15. Andersson, O., Ulrich, C., Bjorefors, F. & Liedberg, B. Imaging SPR for detection of local electrochemical processes on patterned surfaces. *Sens. Actuators B* **134,** 545–550 (2008).
16. Shan, X. N., Patel, U., Wang, S. P., Iglesias, R. & Tao, N. J. Imaging local electrochemical current via surface plasmon resonance. *Science* **327,** 1363–1366 (2010).
17. Foley, K. J., Shan, X. & Tao, N. J. Surface impedance imaging technique. *Anal. Chem.* **80,** 5146–5151 (2008).
18. Giaever, I. & Keese, C. R. Micromotion of mammalian cells measured electrically. *Proc. Natl Acad. Sci. USA* **88,** 7896–7900 (1991).
19. Urdapilleta, E., Bellotti, M. & Bonetto, F. J. Impedance analysis of cultured cells: a mean-field electrical response model for electric cell-substrate impedance sensing technique. *Phys. Rev. E* **74,** 041908 (2006).
20. Bremer, E., van Dam, G., Kroesen, B., de Leij, L. & Helfrich, W. Targeted induction of apoptosis for cancer therapy: current progress and prospects. *Trends Mol. Med.* **12,** 382–393 (2006).
21. Hougardy, B. M. T. *et al.* Proteasome inhibitor MG132 sensitizes HPV-positive human cervical cancer cells to rhTRAIL-induced apoptosis. *Int. J. Cancer* **118,** 1892–1900 (2006).
22. Aihara, H. & Miyazaki, J.-I. Gene transfer into muscle by electroporation *in vivo*. *Nature Biotechnol.* **16,** 867–870 (1998).
23. Olofsson, J. *et al.* Single-cell electroporation. *Curr. Opin. Biotechnol.* **14,** 29–34 (2003).
24. Keese, C. R., Wegener, J., Walker, S. R. & Giaever, I. Eletrical wound-healing assay for cells *in vitro*. *Proc. Natl Acad. Sci. USA* **101,** 1554–1559 (2004).
25. Huang, B., Yu, F. & Zare, R. N. Surface plasmon resonance imaging using a high numerical aperture microscope objective. *Anal. Chem.* **79,** 2979–2983 (2007).

Acknowledgements

The authors thank the National Institutes of Health (NIH, R21RR026235) and National Science Foundation (NSF, CHE-0554786) for support.

Author contributions

K.F. performed initial impedance imaging of cells. W.W. carried out the measurement and data analysis presented here. X.S. contributed to numerical simulation and prepared gold chips. S.E., V.J.N. and P.W. helped with cell culture. K.F. and U.P. developed imaging processing software. W.W., K.F. and S.W. designed and set up the experiment. N.J.T. conceived the experiment and model simulation, and wrote the paper.

Additional information

The authors declare no competing financial interests. Supplementary information accompanies this paper at www.nature.com/naturechemistry. Reprints and permission information is available online at http://npg.nature.com/reprintsandpermissions/. Correspondence and requests for materials should be addressed to N.J.T.